

Features of structural changes in mosaic Ge:Sb according to X-ray diffractometry and electron backscatter diffraction data

M.D. Borcha^{1*}, M.S. Solodkyi¹, S.V. Balovskyak¹, V.M. Tkach², I.I. Hutsuliak¹, A.R. Kuzmin¹, O.O. Tkach¹, V.P. Kladko³, O.Yo. Gudymenko³, O.I. Liubchenko³, Z. Świątek⁴

¹*Yu. Fedkovych Chernivtsi National University,*

²*Kotsyubinskiy str., 58012 Chernivtsi, Ukraine*

²*V. Bakul Institute of Superhard Materials, NAS of Ukraine,*

²*Avtozavodska str., 03142 Kyiv, Ukraine*

³*V. Lashkaryov Institute of Semiconductor Physics, NAS of Ukraine,*

⁴¹*prospect Nauky, 03680 Kyiv, Ukraine*

⁴*Institute of Metallurgy and Materials Science, Polish Academy of Science, Krakow, Poland*

*Corresponding author e-mail: m_borcha@ukr.net

Abstract. The structural homogeneity and degree of perfection inherent to mosaic Ge:Sb samples were investigated. The modified methods for analyzing diffraction images of backscattered electrons (Kikuchi patterns) were used to reduce the influence of instrumental factors. The root-mean-square deformations in the local regions of separate grains and at the boundaries between them were determined using the value of the spatial frequency of the energy spectrum of two-dimensional Fourier transform of Kikuchi patterns. It is shown that the maximum values of deformations ($\sim 3.5 \cdot 10^{-3}$) are typical for local regions, which are usually located at the boundaries between subgrains. X-ray studies confirm obtained values of root-mean-square deformations.

Keywords: high resolution X-ray diffractometry, electron backscatter diffraction, Kikuchi method, reciprocal space maps, Fourier transform.

<https://doi.org/10.15407/spqeo22.04.381>

PACS 61.05.cp, 61.05.J-, 61.72.Dd, 61.05.jm, 61.72.Mm, 61.72.uf, 68.35.Gy

Manuscript received 24.07.19; revised version received 10.09.19; accepted for publication 29.10.19; published online 08.11.19.

1. Introduction

Germanium is one of the most widespread materials for detectors in the infrared spectral range, which is due to good combination of optical, mechanical, physical, chemical, and technological properties [1-5]. Nowadays, Ge doped with Na or Sb with the concentrations $n = 1 \times 10^{13} \dots 5 \times 10^{14} \text{ cm}^{-3}$ has promising applications in electronics and optics [6]. At the same time, there is a decrease in crystal transparency in the infrared spectral range of radiation outside of this range of concentrations, in particular, when $n < 1 \times 10^{13} \text{ cm}^{-3}$, the transparency decreases due to absorption of radiation during carrier transition between the subbands of the valence band, and at the concentrations above $n > 5 \times 10^{14} \text{ cm}^{-3}$ due to the increased scattering of radiation by free electrons [6-8]. In most cases, Ge:Sb crystals are heterogeneous and mosaic. The reason for this can be the heterogeneous distribution of impurities, high dislocation densities, as well as the presence of residual thermoelastic stresses caused by the applied crystal growth technology.

Nowadays, there are a large number of different methods for studying defect system and structure of mono- or polycrystalline crystal materials [9-21]. In particular, the method of electron backscatter diffraction (EBSD or the Kikuchi method) is efficient for determining local structural homogeneity of monocrystalline materials, polycrystalline films and multilayer structures [13-21] and also makes it possible to determine crystallographic orientation of grains and angular orientation between them [13, 18]. At the same time, using the X-ray methods one can determine the integrated values of strain, angular misorientation between individual fragments of the structure, bending radius of atomic planes etc. [9, 11].

In this paper, a modified method for analyzing EBSD images (Kikuchi patterns) was used to study the planar structural homogeneity of mosaic Ge:Sb crystals. The analysis of parameters of the energy spectrum of a two-dimensional Fourier transformation in this method was performed for determining the root-mean-square deformations in the local regions of individual grains and

at the boundaries between them [20]. At the same time, investigation were carried out using high-resolution X-ray diffractometry to obtain the integral characteristics of the structural perfection of Ge:Sb samples.

2. Objects of research

The technology of obtaining Ge:Sb is described in the paper [6]. Polycrystalline Ge was used as an initial material. Growing the sample was carried with the device like "Redmet-10M" by pulling the melt out by using a single-crystal seed. An alloy of Ge with Sb was added to the starting material placed in a graphite pot and melted at the temperature 970 °C. The rate of pulling the crystal from the melt was 1.0 mm/min. The concentration of electrically active dopant atoms in the crystals was $(4\dots 6)\times 10^{13} \text{ cm}^{-3}$. The presence of Sb impurities was determined using a neutron activation analysis.

3. Experimental part

Experimental studies of mosaic Ge:Sb samples were carried out using the Panalytical Philips X'Pert PRO diffractometer for $\text{CuK}_{\alpha 1}$ radiation and scanning electron microscope Zeiss EVO-50 with CCD detector.

3.1. X-ray diffractometry

A high-resolution set with a parabolic mirror, located behind the X-wave tube with $\text{CuK}_{\alpha 1}$ radiation, followed by a four-crystal monochromator Bartels ($4\times\text{Ge}220$) and a point detector with a triple crystal analyzer ($3\times\text{Ge}220$) was used for X-ray studies. The difference between the primary beam and the angular acceptance of the crystal analyzer used before the detector was $\Delta\alpha_{i,f}\approx 12$ angular seconds.

Fig. 1a shows reciprocal space maps (RSM) obtained for one of the largest Ge grain with asymmetric reflection. The cross-sections of RSM (along Q_x axis, which corresponds to the rocking curve, and along Q_z axis, which corresponds to the diffraction curve) are analyzed to obtain more detailed information about the defective structure of the samples.

The presence of additional peaks on the RSM (Fig. 1a) and on the rocking curve $I_h(\omega)$ (Fig. 2) indicates the presence of separate blocks, and peaks' intensity and distance between them – the size and angular orientation. In particular, the misorientation (tilt) between the largest blocks is $1\dots 3^\circ$. The blocks are imperfect, since all the maxima are characterized by a significant angular FWHM, which on average has the order of hundreds angular seconds. The lattice parameter of the largest grain is $a = 5.6577 \text{ \AA}$. The diffuse part of RSM $I_h(\omega, 2\theta-\omega)$ of the main grain is shifted to the negative region along Q_z axis. This may indicate a slight tensile strain in the block.

The change of rocking curve FWHM is caused by the structural imperfections of crystal, angular width of reflection of monochromator and sample, and geometric factors [10, 11]. Determination of the contribution of each component to the change in the shape of the rocking curve can be carried out in different ways. If the shape of $I_h(\omega)$ is described by the Gaussian distribution, then the

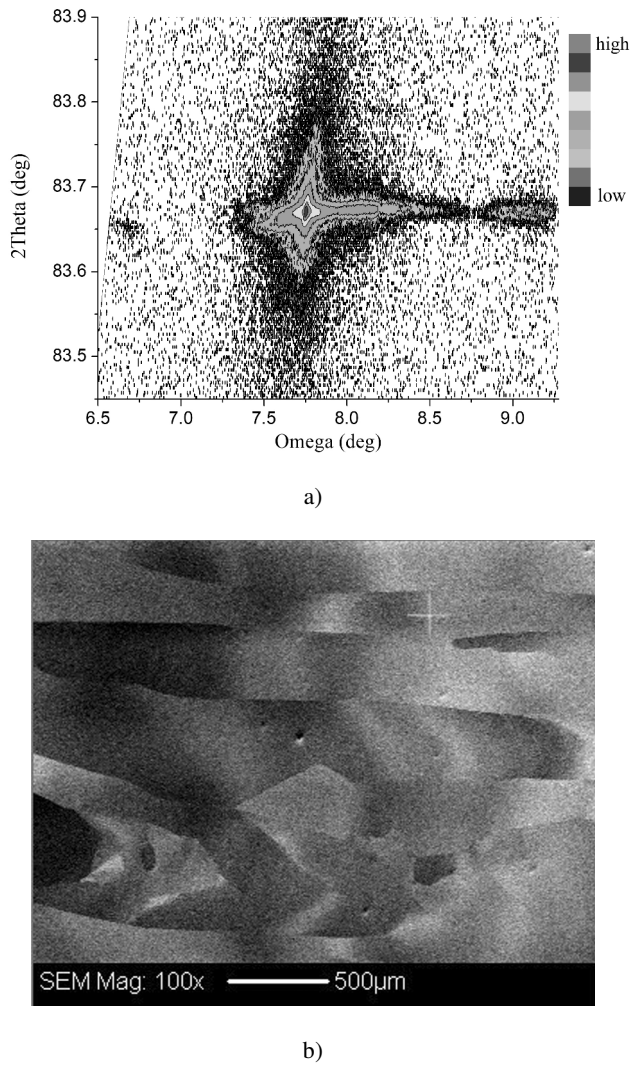


Fig. 1. Sample Ge:Sb, $\text{CuK}_{\alpha 1}$ 224 reflection. Reciprocal space map, built in the coordinates of scanning angles ω and 2θ (a), and a part of the topographic image of Ge structure from EBSD (b).

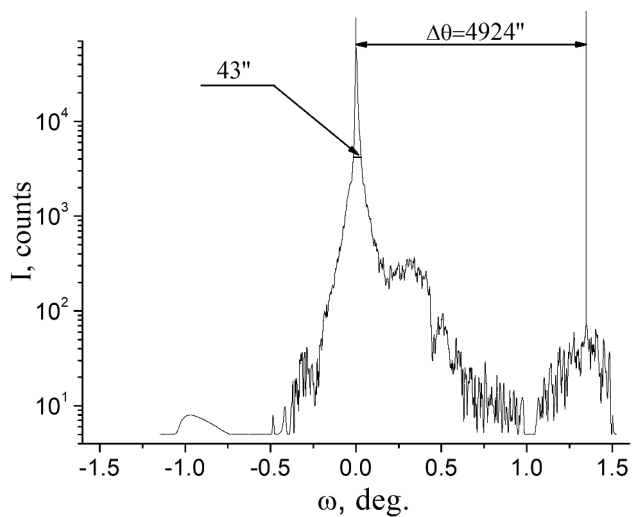


Fig. 2. Experimental rocking curve $I_h(\omega)$, $\text{CuK}_{\alpha 1}$ 224 reflection.

influence of the defective component, which depends on the density of dislocations and stacking faults W_G , is determined from the equation [10, 22]:

$$W_{\text{exp}} = \sqrt{W_G^2 + W_{\text{theor}}^2}, \quad (1)$$

where $W_{\text{theor}} = \frac{2C|\chi_h|}{\sin 2\theta}$, χ_h is the Fourier component of crystal polarization, C – polarization factor. In particular, for 224 reflexes $W_{\text{theor}} = 10.98''$, $W_{\text{exp}} = 43.15''$.

Eq. (1) gives a quantitative estimation of the physical increase of FWHM of the rocking curve (W_G) due to the integral effect of various types of defects in the crystal, including dislocations. In the case of a chaotic dislocation distribution, which occurs in real crystals, the average dislocation density can be estimated from the equation [22]:

$$N_G = \frac{W_G^2}{9|\vec{b}|^2}, \quad (2)$$

where \vec{b} is the Burgers vector of dislocation.

The estimated dislocation density for studied Ge:Sb sample, obtained from Eq. (2), is $N_G \sim 3.0 \times 10^6 \text{ cm}^{-2}$. It results in the average relative deformation in a separate block $\bar{\epsilon}_x \approx 8.7 \times 10^{-4}$. This $\bar{\epsilon}_x$ value can be explained by the presence of a wide complex of defects, as well as, in particular, by the difference in values of the covalent Ge and Sb radii, which are equal to 1.22 and 1.38 Å, respectively. It can lead to formation of a significant amount of micro-inhomogeneities (for example, spherical or prismatic forms of cluster formations) in the crystal bulk and cause fragmentation under certain technological conditions (in particular, with a temperature gradient that is non-uniform along crystallization front and, as a result, an inhomogeneous impurity distribution).

It should be noted that the estimated values of N_G do not quite correlate with the results of work [6], where the dislocation density is $\sim 2.4 \times 10^5 \text{ cm}^{-2}$ for the same Ge:Sb samples obtained from metallographic studies.

3.2. The EBSD method (Kikuchi method)

Kikuchi images (Fig. 3b) were obtained for different parts of the samples under study by using an electron beam with the diameter close to 40 nm, the angle of incidence was 70° (Fig. 3a).

The obtained diffraction patterns (Fig. 3b) confirm the inhomogeneity and crystalline imperfection of the sample. The part of the sample surface (Fig. 3a) has grains of various sizes with a slight angular misorientation. Fig. 1b also shows separate grains with a higher angular misorientation ($>1^\circ$) between adjacent blocks.

The differences between the Kikuchi images for different areas of the sample depend not only on the structural characteristics of the crystals under study, but also on the experimental conditions (displacement and scaling in width and height, rotation, change in intensity and contrast). The diffraction patterns pass several stages of digital processing to exclude such an influence.

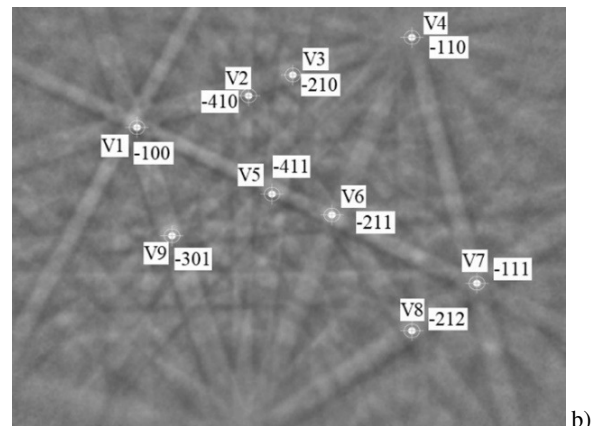
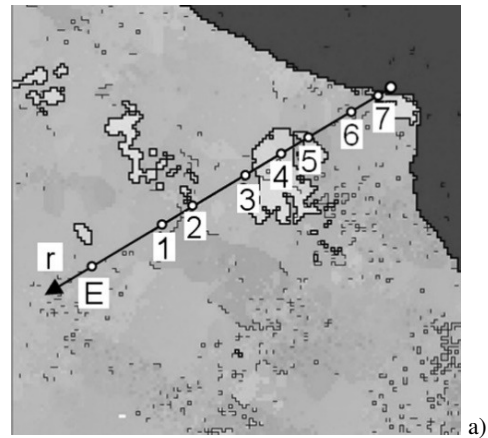


Fig. 3. a) Part (1242×1210 µm) of cathodoluminescent image of Ge surface. Markers indicate the areas No 1 – No 7 and etalon area No 0 (E), for which Kikuchi patterns were obtained; b) Kikuchi pattern of etalon area E. The markers indicate the indices of zone axes and the nodes between which the intensity profiles of the Kikuchi bands were determined.

In particular, the comparison of the Kikuchi images No 1 – No 7 with the etalon image (E) was performed using the genetic algorithms [20, 23, 24]. Since the degree of blurring of the Kikuchi patterns obtained from different regions of the crystal varies significantly, it was expedient to analyze the Kikuchi patterns using the methods of two-dimensional Fourier transform and the Fourier energy spectrum [20]. Image processing was performed with MatLab software [25, 26].

Crystal deformations $\Delta d/d$ (Fig. 4) (relative changes of interplanar distances) can be determined analyzing the area changes under the Kikuchi band intensity profile ε_S , and on the basis of radial distributions P_R of Kikuchi image energy spectra [20, 24]. Deformations ε_T and ε_A are found through the changes of average radial period \bar{T}_r (3) and the radial distribution area S_{PR} (4) of the radial distribution P_R , respectively:

$$\varepsilon_T = k_T \cdot \ln \left(\frac{\bar{T}_{r0}}{\bar{T}_r} \right), \quad (3)$$

$$\varepsilon_A = k_S \cdot \ln \left(\frac{S_{P_R}}{S_{P_{RM}}} \right), \quad (4)$$

where the coefficients $k_T = 4.33 \times 10^{-3}$ and $k_S = 1.4 \times 10^{-3}$ are chosen by minimization of the average square difference between ε_A and ε_S ; \bar{T}_r are the average radial periods for the regions No 1 – No 7; \bar{T}_{r0} is the average radial period for the etalon region No 0 (E); S_{PR} are the areas of radial distribution P_R for the regions No 1 – No 7; S_{PRM} is the area for radial distribution P_R for the etalon region No 0 (E).

Values ε_T and ε_A in Fig. 4 are consistent with the strain values ε_S , obtained on the basis of our analysis of changes in the profiles of the bands. The lowest values of ε_A , ε_T and ε_S are characteristic for local areas No 6 and No 7. The highest – for local areas No 1, No 2 and No 3, which, as a rule, are located on the borders (or near them) between the subgrains (Fig. 3a). In particular, $\varepsilon_S \approx 1.5 \times 10^{-3}$, $\varepsilon_A \approx \varepsilon_T \approx 2.0 \times 10^{-3}$ for the etalon area; $\varepsilon_A \approx \varepsilon_T \approx \varepsilon_S \approx 3.5 \times 10^{-3}$ are the highest for area No 2; $\varepsilon_A \approx \varepsilon_T \approx \varepsilon_S \approx 0.5 \times 10^{-4}$ are the lowest for area No 7. In general, it is confirmed by X-ray studies (Figs. 1a and 2).

The existing difference for the regions No 1 and No 4 (Fig. 4) in the ε_T , ε_A and ε_S values can be explained by different approaches to their definition. The value ε_S is more influenced by anisotropy in the distribution of deformations, since it is associated not only with changes in the geometry of the bands as well as with their crystallographic orientation [24]. In our case, ε_S values shows that the Kikuchi band profiles are the least blurred in regions No 1 and No 4 and close in their shape to the same ones from the etalon region (E).

At the same time, satisfactory consistency between these ε_T , ε_A and ε_S values in Fig. 4 shows that the complex use of various approaches during the analysis of Kikuchi images increases the reliability of the obtained results and indicates the prospect of using the Fourier energy spectrum.

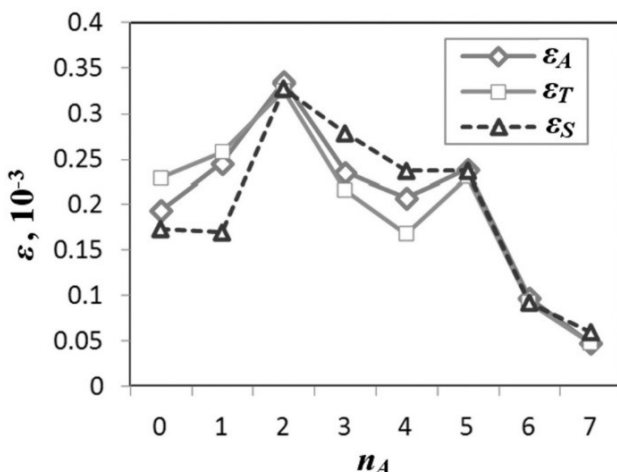


Fig. 4. Diagram of the average strain deformation in local regions of mosaic Ge:Sb, calculated using different methods; ε_A – deformations calculated based on the radial distribution area P_R ; ε_T – deformations calculated on the basis of the average radial period \bar{T}_r ; ε_S are the average deformations calculated on the basis of Kikuchi bands profiles.

Consequently, the complex use of the methods of high-resolution X-ray diffraction and EBSD method to determine the degree of structural perfection of mosaic Ge:Sb allows us to get not only the value of averaged deformations and the limits of angular misorientation between individual fragments, but also to obtain the distribution of average strain values in separate blocks and at the boundaries between them, and also to reveal crystallographic directions with the smallest (or largest) values of averaged deformations.

4. Conclusions

1. The complex use of the methods based on high resolution X-ray diffractometry and modified method for analyzing the parameters of the energy spectrum of a two-dimensional Fourier transformation for the Kikuchi patterns create additional opportunities for determination of the influence of technological parameters on the structural homogeneity and the degree of perfection of mosaic and polycrystalline specimens.

2. The estimated values of dislocation densities obtained by the analysis of RSM and rocking curve of Ge:Sb samples are $N_G \sim 3.0 \times 10^6 \text{ cm}^{-2}$. This density of dislocations causes the average relative deformation – $\bar{\varepsilon}_x \approx 8.7 \times 10^{-4}$ in a single block. The same values of averaged deformations (in order) are obtained from the analysis of Kikuchi images by various methods.

3. The value of the spatial frequency of the radial distributions of the energy spectrum is calculated for the whole image, which reduces the influence of the distortions of the experimental Kikuchi patterns and makes it possible to determine the difference in the value of root-mean-square deformations in the local regions of individual grains and at the boundaries of their division more precisely. The lowest values of ε_A , ε_T and ε_S are characteristic for local areas No 6 and No 7. The highest – for local areas No 1, No 2 and No 3, which, as a rule, are located on the borders (or near them) between the subgrains (Fig. 3a). In particular, $\varepsilon_S \approx 1.5 \times 10^{-3}$, $\varepsilon_A \approx \varepsilon_T \approx 2.0 \times 10^{-3}$ for the etalon area; $\varepsilon_A \approx \varepsilon_T \approx \varepsilon_S \approx 3.5 \times 10^{-3}$ are the highest for area No 2; $\varepsilon_A \approx \varepsilon_T \approx \varepsilon_S \approx 0.5 \times 10^{-4}$ are the lowest for area No 7.

4. The average deformations ε_T and ε_A calculated on the basis of the analysis of the energy spectrum parameters correlates well with the values of deformations ε_S , obtained on the basis of the Kikuchi band profiles. The complex use of various approaches to the analysis of Kikuchi images increases reliability of the obtained data.

References

1. Claeys C., and Simoen E. *Germanium-based Technologies: From Materials to Devices*. Berlin, Elsevier, 2007.
2. Koester S.J., Schaub J.D., Dehlinger G., and Chuijee J.O. Germanium-on-SOI infrared detectors for integrated photonic applications. *IEEE J. Sel.*

- Top. Quantum Electron.* 2006. **12**, No 6. P. 1489–1502. <https://doi.org/10.1109/JSTQE.2006.883160>.
3. Olson J., Kurtz S., Kibbler A. and Faine A. A 27.3% efficient $\text{Ga}_{0.5}\text{In}_{0.5}\text{P}/\text{GaAs}$ tandem solar cell. *Appl. Phys. Lett.* 1990. **56**, No 7. P. 623–625. <https://doi.org/10.1063/1.102717>.
 4. King R.R., Law D.C., Edmondson K.M. et al. 40% efficient metamorphic $\text{GaInP}/\text{GaInAs}/\text{Ge}$ multi-junction solar cells. *Appl. Phys. Lett.* 2007. **90**, No 18. P. 183516. <https://doi.org/10.1063/1.2734507>.
 5. Raoux S., Cheng H., Jordan-Sweet Jean L., Munoz B., and Hitzbleck M. Influence of interfaces and doping on the crystallization temperature of Ge–Sb. *Appl. Phys. Lett.* 2009. **94**, No 18. P. 183114. <https://doi.org/10.1063/1.3133344>.
 6. Pat. 81729 Ukraine, CI C30B 15/00, C30B 29/08, C30B 33/02. Optical germanium. H.S. Pekar, O.F. Synhayivs'kyy – 29.11.2006; publ. 25.01.2008, Bul. №19.
 7. Kaplunov I.A., Kolesnikov A.I., and Shaiovich S.L. Methods for measuring light scattering in germanium and paratellurite crystals. *Crystallography Reports.* 2005. **50**, No 1. P. S46–S52. <https://doi.org/10.1134/1.2133971>.
 8. Astaf'ev N.I., Nesmelova I.M., Nesmelov E.A. Features of semiconductor materials as infrared optical media. *J. Opt. Technol.* 2008. **75**, No 9. P. 608–610. <https://doi.org/10.1364/JOT.75.000608>.
 9. Ludwig W., Schmidt S., Lauridsen E., and Poulsen H. X-ray diffraction contrast tomography: a novel technique for three-dimensional grain mapping of polycrystals. I. Direct beam case. *J. Appl. Crystallogr.* 2008. **41**, No 2. P. 302–309. <https://doi.org/10.1107/S0021889808001684>.
 10. Bowen D. and Tanner B. *High Resolution X-Ray Diffractometry and Topography*. CRC Press, 1998.
 11. Authier A. *Dynamical Theory of X-Ray Diffraction*. New York, Oxford University Press, 2001. <https://doi.org/10.1093/acprof:oso/9780198528920.001.0001>.
 12. Holy V., Pietsch U. and Baumbach T. *High-Resolution X-ray Scattering from Thin Films and Multilayers*. Heidelberg, Springer, 1999. <https://doi.org/10.1007/BFb0109385>.
 13. Fodchuk I.M., Balovskyak S.V., Borch M.D., Garabazhiv Ya.D., and Tkach V.N. Determination of structural homogeneity of synthetic diamonds from analysis of Kikuchi lines intensity distribution. *SPQEO*. 2010. **13**, No 3. P. 262–267.
 14. Wilkinson A. and Britton B. Strains, planes, and EBSD in materials science. *Materials Today*. 2012. **15**, No 9. P. 366–376. [https://doi.org/10.1016/S1369-7021\(12\)70163-3](https://doi.org/10.1016/S1369-7021(12)70163-3).
 15. Stoll A. and Wilkinson A.J. Simulation of deformation twins and their interactions with cracks. *Comput. Mater. Sci.* 2014. **89**. P. 224–232. <https://doi.org/10.1016/j.commatsci.2014.03.041>.
 16. Dingley D.J., Wilkinson A.J., Meaden G., and Karamched P.S. Elastic strain tensor measurement using electron backscatter diffraction in the SEM. *J. Electron Microscopy*. 2010. **59**, No S1. P. S155–S163. <https://doi.org/10.1093/jmicro/dfq043>.
 17. Borch M., Zvyagintseva A., Tkach V. et al. Local deformations in the vicinity of welded-joint crack of nickel alloy determined with use of Fourier transform of the Kikuchi patterns. *Metallofizika Noveishie Tekhnol.* 2013. **35**, No 10. P. 1359–1370.
 18. Borch M., Balovskyak S., Fodchuk I., Khomenko V., and Tkach V. Distribution of local deformations in diamond crystals according to the analysis of Kikuchi lines profile intensities. *J. Superhard Materials.* 2013. **35**, No 4. P. 220–226. <https://doi.org/10.3103/S1063457613040035>.
 19. Fodchuk I., Balovskyak S., Borch M., Garabazhiv Ya., and Tkach V. Determination of structural inhomogeneity of synthesized diamonds by backscattering electron diffraction. *phys. status solidi (a)*. 2011. **208**, No 11. P. 2591–2596. <https://doi.org/10.1002/pssa.201184266>
 20. Fodchuk I., Solodkyi M., Borch M., Balovskyak S., and Tkach V. Determination of local deformations and their anisotropy in polycrystalline Ge by electron backscatter diffraction data. *Metallofizika Noveishie Tekhnol.* 2019. **41**, No 3. P. 403–415. <https://doi.org/10.15407/mfint.41.03.0403>.
 21. Fodchuk I., Tkach V., Ralchenko V. et al. Distribution in angular mismatch between crystallites in diamond films grown in microwave plasma. *Diamond Relat. Mater.* 2010. **19**, No 5–6. P. 409–412. <https://doi.org/10.1016/j.diamond.2010.01.020>.
 22. Hirt P. *Mosaic Structure*. Moscow, Mir, 1960.
 23. Balovskyak S., Fodchuk I. Objects images alignment with the use of genetic and gradient algorithms. *Computing*. 2013. **12**, No 2. P. 160–167.
 24. Borch M., Solodkyi M., Balovskyak S. et al. Determination of local strains in a neighborhood of cracks in a welded seam of Ni-Cr-Fe according to the power Fourier spectrum of Kikuchi patterns. *Physics and Chemistry of Solid State*. 2018. **19**, No 4. P. 307–312. <https://doi.org/10.15330/pcss.19.4.307-312>.
 25. Gonsales R., Woods R., and Eddins S. *Digital Image Processing using MATLAB*. Moscow, Tekhnosfera, 2006.
 26. Gonsales R. and Woods R. *Digital Image Processing*. Moscow, Tekhnosfera, 2005.

Authors and CV



Borcha M.D. defended her Doctoral Dissertation (Physics of Solid State) in 2013. Scientific supervisor of project of the Applied and Fundamental Research of Ukraine. Authored over 50 publications. The area of her scientific interests includes the strain distribution in real crystals determined using the methods of electron backscatter diffraction and multi-beam X-ray diffraction in semiconductor crystals, hetero- and nanosystems.



Solodkyi M.S. Postgraduate student of the Yu. Fedkovych Chernivtsi National University. The area of his scientific interests is the strain state in real crystals by the data of electron backscatter diffraction method, material analysis sciences and high-resolution X-ray diffraction. He is author of 3 articles.



Hutsuliak I.I. Defended his Ph.D. dissertation in 2013. The area of his scientific interests includes solid state physics and semiconductor physics. He is the author of 12 publications.



Balovskyak S.V. defended his Ph.D. dissertation in 2003. The area of his scientific interests includes improvement of techniques for the diagnosis of solid surface morphology by methods of complete external reflection of X-rays, including experimental studies and computer processing of the obtained results. Authored over 60 publications.



Kuzmin A.R. Postgraduate student of the Yu. Fedkovych Chernivtsi National University. The area of scientific interests is the X-ray diffraction analysis of semiconductor crystals, hetero- and nanosystems.



Tkach V.M. Doctor of Sciences (Physics and Mathematics), Head of the Laboratory of Nanostructured and Crystal Physical Research at the V. Bakul Institute for Superhard Materials. Authored over 300 publications. The area of scientific interests is the study of structure and spectral characteristics of superhard mono- and polycrystalline materials.



Tkach O.O. Defended her Ph.D. dissertation in 2004. The area of her scientific interests includes solid-state physics, dynamical theory of diffraction of radiation and semiconductor physics. She is the author of 23 publications.



Oleksandr Gudymenko, Ph.D. in Physics and Mathematics, Researcher at the Department of Structural and Elemental Analysis of Materials and Systems at the V. Lashkaryov Institute of Semiconductor Physics. Author of more than 56 publications. His research interests include: solid-state physics, dynamical theory of diffraction of radiation, X-ray optics,



Kladko V.P. Doctor of Sciences (Physics and Mathematics), Corresponding Member of NAS of Ukraine, Head of the Department of Structural and Elemental Analysis of Materials and Systems at the V. Lashkaryov Institute of Semiconductor Physics, NASU. Author of more than 300 publications. His research interests include solid-state physics, dynamical theory of diffraction of radiation, X-ray optics, X-ray diffraction analysis of semiconductor crystals, hetero- and nanosystems.

X-ray diffraction analysis of semiconductor crystals, hetero- and nanosystems, XRD analysis materials, X-ray reflectometry of thin films. E-mail: gudymen@ukr.net ORCID: <https://orcid.org/0000-0002-5866-8084>



Liubchenko O.I. graduated from the National Technical University of Ukraine "Igor Sikorsky Kyiv Polytechnic Institute" in 2015. PhD, researcher at the Department for Diffraction Analysis of the Structure of Semiconductors, V. Lashkaryov Institute of Semiconductor Physics, NASU. The area of scientific interests is analysis of materials science objects, high-resolution X-ray diffraction and computer simulation of XRD spectra. He authored 6 articles.



Świątek Z. Associate Professor at the Institute of Metallurgy and Materials Science, Polish Academy of Sciences. Professor of Polish Academy of Sciences. Scientific achievements: 79 papers in peer-reviewed journals and periodicals, 106 presentations during conferences.